How an alloreactive T-cell receptor achieves peptide and MHC specificity

Yuan Wang[a,b], Nishant K. Singh[a,b], Timothy T. Spear[c,d], Lance M. Hellman[a,b], Kurt H. Piepenbrink[e], Rachel H. McMahan[f], Hugo R. Rosen[f], Craig W. Vander Kooi[g], Michael I. Nishimura[c,d], and Brian M. Baker[a,b,1]

[a]Department of Chemistry and Biochemistry, University of Notre Dame, Notre Dame, IN 46556; [b]Harper Cancer Research Institute, University of Notre Dame, Notre Dame, IN 46556; [c]Department of Surgery, Loyola University Chicago, Maywood, IL 60153; [d]Cardinal Bernardin Cancer Center, Loyola University Chicago, Maywood, IL 60153; [e]Department of Food Science and Technology, University of Nebraska, Lincoln, NE 68588; [f]Division of Gastroenterology & Hepatology, Department of Medicine, University of Colorado School of Medicine, Aurora, CO 80045; and [g]Department of Molecular and Cellular Biochemistry, University of Kentucky, Lexington, KY 40506

T-cell receptor (TCR) allorecognition is often presumed to be relatively nonspecific, attributable to either a TCR focus on exposed major histocompatibility complex (MHC) polymorphisms or the degenerate recognition of allopeptides. However, paradoxically, alloreactivity can proceed with high peptide and MHC specificity. Although the underlying mechanisms remain unclear, the existence of highly specific alloreactive TCRs has led to their use as immunotherapeutics that can circumvent central tolerance and limit graft-versus-host disease. Here, we show how an alloreactive TCR achieves peptide and MHC specificity. The HCV1406 TCR was cloned from T cells that expanded when a hepatitis C virus (HCV)-infected HLA-A2⁻ individual received an HLA-A2⁺ liver allograft. HCV1406 was subsequently shown to recognize the HCV nonstructural protein 3 (NS3):1406–1415 epitope with high specificity when presented by HLA-A2. We show that NS3/HLA-A2 recognition by the HCV1406 TCR is critically dependent on features unique to both the allo-MHC and the NS3 epitope. We also find cooperativity between structural mimicry and a crucial peptide "hot spot" and demonstrate its role, along with the MHC, in directing the specificity of allorecognition. Our results help explain the paradox of specificity in alloreactive TCRs and have implications for their use in immunotherapy and related efforts to manipulate TCR recognition, as well as alloreactivity in general.

T-cell receptor | peptide-MHC | structure | alloreactivity | specificity

T-cell receptor (TCR) recognition of peptides bound and presented by proteins encoded by the major histocompatibility complex (MHC) underlies specificity in cellular immunity. The MHC locus is the most polymorphic region in the human genome, leading to many thousands of expressed MHC variants. Of these MHC variants, any one individual can express, at most, six class I and six class II proteins. Selection processes during thymic education result in a TCR repertoire tolerant of self-peptides presented by self-MHC, as evidenced by the strong immune responses associated with transplantation of tissues with donor/recipient MHC mismatches (alloreactivity). Indeed, precursor frequencies for alloreactive T cells are up to 1,000-fold higher than frequencies for T cells that respond to self-MHC (1). Alloreactive T-cell responses contribute to the significant morbidity associated with rejection of transplanted tissues and graft-versus-host disease.

Surprisingly, many alloreactive T cells display a degree of specificity reflective of traditional syngeneic T cells (2), a counterintuitive finding, given the prevailing theories that alloreactivity is driven by TCR "misfocusing" on non–self-MHC polymorphisms (MHC-centric) or the recognition of a repertoire of unique allopeptides (peptide-centric) (3). Although this enigma has not been fully explained, it has nonetheless led to a growing interest in the use of such "allospecific" TCRs in immunotherapy. Central tolerance mechanisms exist to avoid self-reactivity, hindering the identification of highly avid T cells specific for shared (nonmutated) tumor antigens. The phenomenon of specificity in alloreactivity

has thus been exploited to identify T cells capable of recognizing shared tumor antigens with high potency, using antigen-specific T cells from mismatched donors to circumvent tolerance (4, 5). In a related fashion, antigen-specific alloreactive T cells have been used to target conditions such as posttransplantation Epstein–Barr virus-associated lymphoma (6, 7).

Several studies have examined the structural features of allogeneic TCR–pMHC complexes (8–11). An overall assessment of these structures is that rather than demonstrating features that are clearly characteristic of alloreactivity, they illustrate features similar to traditional syngeneic complexes of TCRs with peptides presented by self-MHC (3, 12, 13). The LC13 TCR, for example, was recently shown to engage allo- and self-MHC almost identically, and could distinguish between closely related class I alleles (14, 15). In that case, recognition of an allopeptide occurred via conformational changes that bring it into a conformation mimicking a viral peptide, thus demonstrating the importance of both the MHC and peptide. A recent study of an alloreactive TCR that specifically recognizes an antigen from Hodgkin's lymphoma concluded that MHC polymorphisms likely determine a unique peptide-binding mode, contributing to high peptide specificity (16). It is clear from these and other studies that specific allorecognition requires elements of the composite peptide-MHC ligand, with the potential for both to influence specificity.

Significance

T-cell alloreactivity drives transplant rejection. Alloreactive recognition is believed to proceed with limited specificity, accounting for the high numbers of alloreactive T cells in humans. Paradoxically, however, many T cells recognize alloantigens with high specificity, and receptors from such T cells are being explored for use in cancer immunotherapy. Here, we explain how a T-cell receptor (TCR) achieves high specificity toward a peptide antigen presented by allo-major histocompatibility complex (MHC). Counter to prevailing theories of alloreactivity, we find that TCR recognition is driven by a cooperative interplay between features unique to both the allo-MHC and the peptide, such that binding is both MHC- and peptide-centric. Our results have broad implications for the determinants of immune recognition and efforts in immunotherapy.

To gain further insight into the paradoxical nature of antigen-specific alloreactivity, we examined an alloreactive human TCR highly specific for the nonstructural protein 3 (NS3):1406–1415 epitope from the hepatitis C virus (HCV) presented by HLA-A2. The HCV1406 TCR was cloned from T cells that expanded when an HCV-infected HLA-A3/A30 individual received an HLA-A2/A24 liver allograft. HLA-A2 and A3/A30 belong to different class I MHC supertypes (17, 18), and A2 has surface properties distinct from HLA-B, HLA-C, nonclassical class I, and the class II proteins. Expression of HCV1406 confers anti-HCV reactivity onto other effector cells, which specifically recognize NS3/HLA-A2 targets independent of the CD8 coreceptor and do not recognize irrelevant targets presented by A2 or other class I MHC proteins (19–22).

In conflict with prevailing theories of T-cell alloreactivity, we show that the specific recognition of NS3/HLA-A2 by HCV1406 is dependent upon three intertwined components: the unique TCR contact surface of A2, including polymorphisms that distinguish it from the other MHC proteins present in the host; the impact of A2 polymorphisms on NS3 peptide binding and conformation; and unique structural and chemical features of the NS3 peptide. Thus, HCV1406 recognition is neither MHC- nor peptide-specific, but is both, emerging from a cooperative interplay of features of the composite peptide-MHC ligand. Our results help explain the paradox of antigen specificity in alloreactivity and have implications for the use of allospecific TCRs in immunotherapy and related efforts to manipulate TCR recognition.

Results

Fine Specificity of the HCV1406 TCR. To help understand the specificity of the HCV1406 TCR and identify the key residues in the NS3 epitope (sequence KLVALGINAV), we performed a mutational scan of the peptide. We assessed the reactivity of HCV1406 TCR-expressing T cells by cytokine secretion when cocultured with HLA-A2$^+$ (referred to as A2) T2 cells pulsed with native NS3:1406–1415 peptide or variants with substitutions at positions 1 through 10. We evaluated the reactivity of TCR-transduced T cells from two normal human donors as well as TCR-transduced CD8$^+$ or CD8-Jurkat E6.1 cells.

The data from the various cell types displayed similar patterns of reactivity (Fig. 1 A and B), with no recognition of nonpeptide-pulsed targets or targets pulsed with the irrelevant tyrosinase:368–376 peptide (sequence YMDGTMSQV). As found previously (19, 20, 22), the TCR specifically recognized NS3/A2 in a CD8-independent manner. Modifications to the peptide had various effects, with alanine substitutions at p1 (Lys) and p6 (Gly) proving the most disruptive. Modification of the leucine at p5 had an intermediate effect, whereas modifications toward the C-terminal end (p8 Asn, p9 Ala, and p10 Val) had little to no impact on recognition. In the experiments with Jurkat cells, the presence of CD8 led to stronger responses as generally anticipated.

To supplement the functional data, we measured the affinity of the HCV1406 TCR toward NS3/A2 in direct binding experiments using surface plasmon resonance (SPR). The TCR bound NS3/A2 with an affinity (K_d) of 16 ± 1 μM (Fig. 1C), which is in the range of other TCRs known to be CD8-independent (23). No binding was again observed with the irrelevant tyrosinase peptide. The affinity to the p1 Lys→Ala (K1A) NS3 variant was measured as ≥170 μM. The large reduction in binding affinity, amounting to a $\Delta\Delta G°$ of ≥1.4 kcal/mol, is consistent with the loss of recognition in the functional experiments. Replacement of the p1 Lys with alanine did not weaken binding of the peptide to A2, as the A2 complexes with both the native NS3 epitope and the K1A variant had identical melting temperatures (T_m values) of 64 °C when measured by differential scanning fluorimetry (DSF) (Fig. 1D), reflective of high-affinity peptide binding (24).

The HCV1406 TCR Binds NS3/HLA-A2 with a Traditional Binding Mode. We determined the structure of the complex between the HCV1406 TCR and the NS3 peptide presented by A2 at a resolution of 2.5 Å (Table 1). The complex crystallized in space group P3121 with two complexes in the asymmetrical unit. Clear
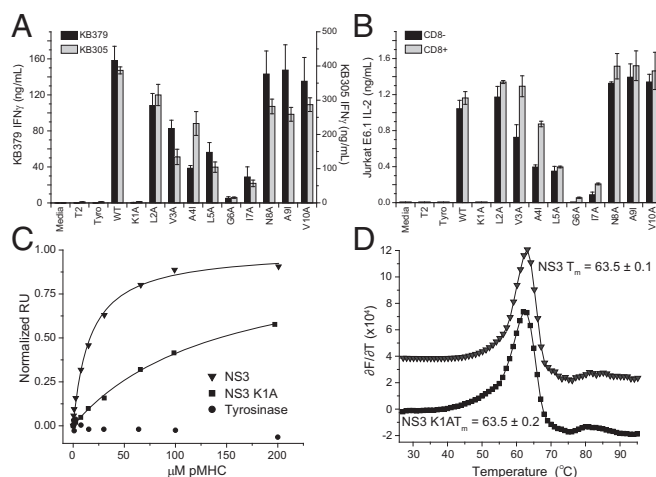
Fig. 1. Fine specificity of the HCV1406 TCR with the NS3 antigen presented by HLA-A2. (A) Cytokine (IFN-γ) release measured with transduced bulk T cells from two donors recognizing peptide-pulsed T2 cells. No response was observed with no peptide or with the irrelevant tyrosinase peptide, whereas strong responses were observed with the native NS3 epitope. Mutations that significantly impacted recognition were K1A and G6A. (B) Cytokine (IL-2) release measured with Jurkat E6.1 cells without CD8 or cotransduced with CD8. The response patterns closely resemble the response patterns with the donor-derived T cells in A. (C) Direct binding of the HCV1406 TCR to NS3/A2 measured by SPR. Binding of the TCR to the native epitope yielded a K_d value of 16 ± 1 μM. Consistent with the functional data, the K1A substitution substantially weakened binding ($K_d ≥ 170$ μM), and no binding was detected with the irrelevant tyrosinase peptide. RU, resonance units. (D) NS3 peptide binds to A2 with high affinity as measured by DSF ($T_m = 63.5$ °C). Substitution of the p1 Lys with Ala did not weaken peptide binding (note the y axis is shifted by +4 units for the K1A data to facilitate comparison with the native peptide data).

electron density was observed for the TCR–pMHC interfaces in both complexes (Fig. S1). The two complexes were essentially identical: All atoms of the peptides superimposed with an rmsd of 0.8 Å, the A2 backbones superimposed with an rmsd of 0.7 Å, and the TCR backbones superimposed with an rmsd of 0.5 Å. The TCR adopts a typical diagonal orientation over the pMHC, binding directly over the peptide-binding groove with a crossing angle of 30° (Fig. 2 A and B). The incident angle (or tilt, defined as the angle between the plane of the MHC peptide-binding groove and a vertical line down the Vα/Vβ pseudosymmetry axis) is 17°. This combination of crossing and incident angles places the docking geometry of HCV1406 near the edge of what has been observed for other A2-binding TCRs (Fig. 2C). However, similar binding angles have been observed with other TCRs (25), and considered alongside the larger set of all human and mice complexes with class I or class II MHC, the binding geometry of HCV1406 is well within what has been observed for functioning TCRs (Fig. S2). The nondistinctive geometry is particularly clear when it is considered alongside TCRs that bind with "reverse polarity" (26, 27) and the nonsignaling 42F3 TCR in complex with the p3A1 ligand (28). As a further demonstration of its traditional binding geometry, the binding of HCV1046 to NS3/A2 was not distinctive when the position of the center of mass of the Vα/Vβ domains over A2 was compared with other A2-binding receptors (Fig. 2D). Although HCV1406 recognition of NS3/A2 is CD8-independent, the binding geometry is compatible with CD8 binding, because naturally occurring NS3 variants require CD8 for efficient recognition by HCV1406-transduced T cells (20), and as shown in Fig. 1B, the presence of CD8 strengthened the responses to single-amino acid NS3 variants.

A total of 2,049 Å^2 of solvent accessible surface area is buried in the TCR–pMHC interface, with 54% contributed by Vα and 46% by Vβ. The TCR buries 345 Å^2 of peptide surface area, or 82% of the peptide surface exposed in the free pMHC complex.

**Table 1. X-ray data collection and refinement statistics**

Data collection	
Resolution, Å	37.2–2.50 (2.6–2.5)
Space group	P 31 2 1
Cell dimensions	
a, b, c; Å	128.8, 128.8, 223.6
α, β, γ; °	90.0, 90.0, 120.0
Unique reflections*	74,525 (7,352)
R_{merge}	0.23 (0.7)
$\langle I/\sigma(I)\rangle$	9.1 (2.9)
Data completeness, %	99.6 (99.2)
Temperature, K	100
Wavelength, Å	1.0
Refinement statistics	
R_{work}/R_{free}†	0.20/0.23
No. of protein atoms	13,339
Rmsd from ideality	
Bond lengths, Å	0.015
Bond angles, °	0.89
Ramachandran statistics, %	
Favored	95
Allowed	5
Outlier	0.1
Average B factors, Å^2	
TCR	56.7
MHC/β_2m	86.8
Peptide	50.6
PDB ID code	5JZI

*Values in parentheses are statistics of the highest resolution shell.
†R_{free} is calculated for a randomly selected 5.0% of reflections not included in refinement.

The complementarity-determining region (CDR) loops are arranged over the pMHC as commonly observed, with the hypervariable CDR3α/CDR3β loops over the center of the peptide; the CDR1α and CDR1β loops over the peptide N- and C-terminal regions, respectively; and the CDR2α and CDR2β loops over the α2 and α1 helices, respectively (Fig. 2B). Using a cutoff distance of 4 Å, there are 134 interatomic contacts in the interface, of which 54 are between the TCR and the peptide and 80 are between the TCR and A2.
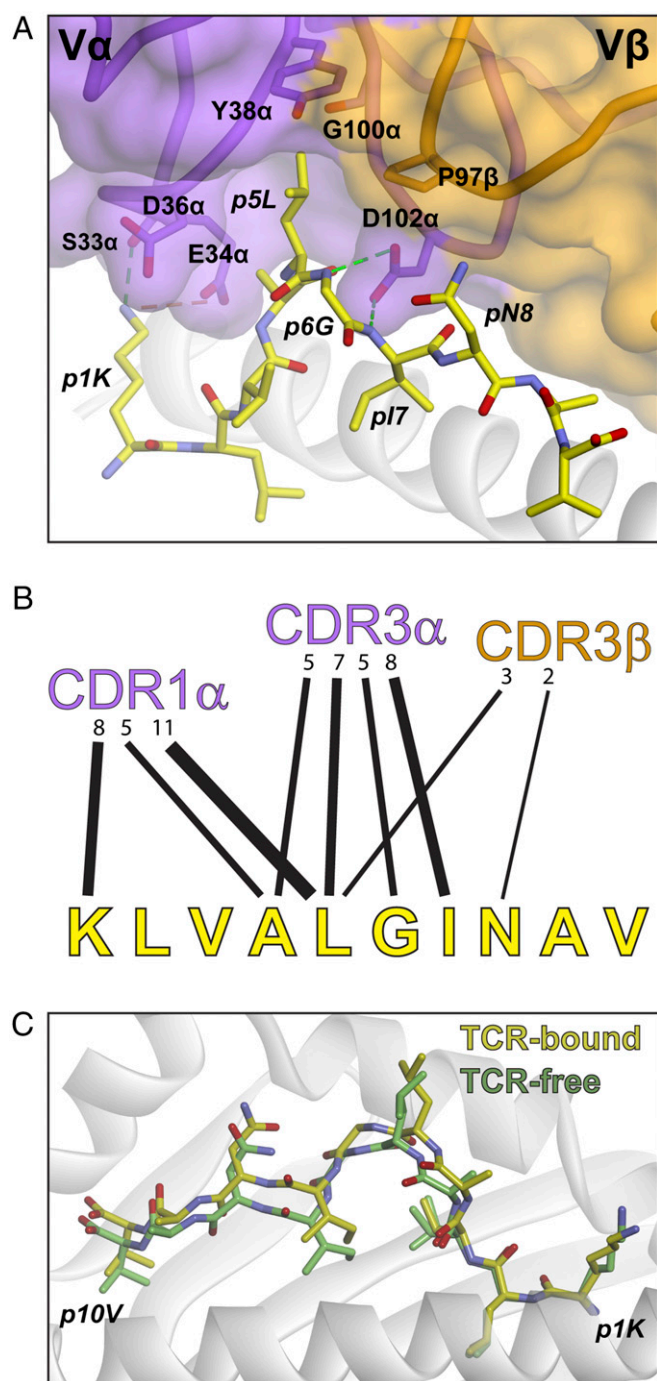
HCV1406 Engagement of the NS3 Peptide. The HCV1406 TCR engages the NS3 peptide along its entire length, although with greater participation of the N-terminal half and the TCR α-chain (Fig. 3 A and B). The protruding side chains of the peptide are the lysine at p1, the leucine at p5, and the asparagine at p8. The p1 Lys is engaged by Ser33 and Glu34 of CDR1α, which form hydrogen bonds and a salt-bridge with the lysine side chain. The p5 Leu fits into a large hydrophobic cleft formed by residues in CDR1α, CDR3α, and CDR3β. The p8 Asn forms only two contacts with CDR3β. Other contacts are hydrogen bonds made to the peptide backbone at p6 and p7 by Asp102 of CDR3α.

The structural data allow a more detailed interpretation of the specificity and binding experiments shown in Fig. 1. The electrostatic interactions with p1 Lys are clearly crucial for recognition, given that substitution of p1 Lys with alanine is the most detrimental peptide modification studied. The loose accommodation of the p5 Leu side chain in the hydrophobic cleft is consistent with the more moderate impact the p5 Leu→Ala substitution has on recognition. The TCR's structural bias toward the N-terminal half of the peptide is consistent with the minor impacts of substitutions at positions 8–10 in recognition. The disruption from substitution of the alanine at p6 Gly is attributable to tight packing between the side of the peptide and residues of the A2 α2-helix, such that mutation of p6 Gly to anything other than alanine is likely to influence peptide conformation.
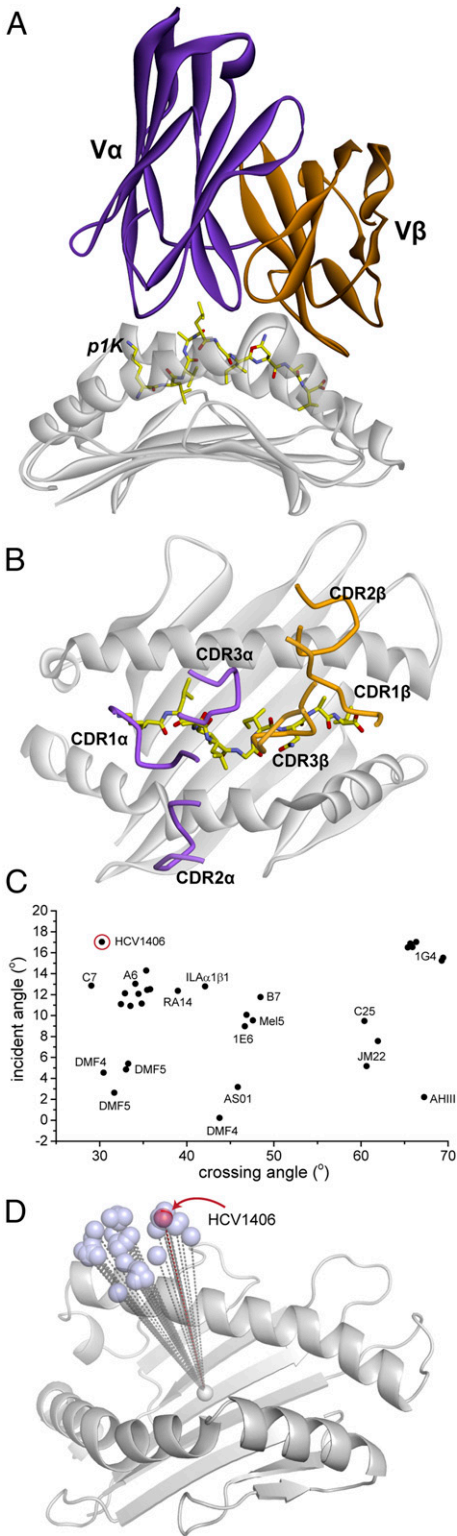
Fig. 2. Overview of the HCV1406–NS3/A2 complex. (A) Structural overview showing the position of the TCR variable domains relative to the pMHC. (B) Position of the CDR3 loops over the A2 molecule. (C) Incident vs. crossing angles for TCRs that bind A2. HCV1406 binds NS3/A2 near the edge as indicated by the red circle, but the docking geometry is within the limits of what has been observed with other receptors (also Fig. S2). (D) Positions of the centers of mass of the Vα/Vβ domains of the A2-binding TCRs in C over the A2 center of mass, with the center of mass of HCV1406 shown in red.

Fig. 3. Engagement of NS3 peptide by HCV1406. (*A*) Key contacts to the peptide from the loops of the Vα and Vβ domains. The side chain of p1 Lys forms a hydrogen bond with Ser33 and a salt-bridge with Glu34 of CDR1α. The side chain of p5 Leu is accommodated by a hydrophobic cleft formed by CDR1α, CDR2α, and CDR3β. Hydrogen bonds are formed to the backbone at positions 6 and 7 by Asp102 of CDR3α. The side chain of p8 Asn is at the edge of the interface, interacting minimally with CDR3β. (*B*) Schematic showing TCR contacts to peptide amino acids by the participating CDR loops. The width of the black lines is proportional to the number of contacts, as indicated by the numbers above each line. (*C*) Comparison of the conformation of the NS3 peptide in the A2-binding groove in the TCR-bound and TCR-free structures. When bound to the TCR, the peptide is "lifted" by ~1 Å, beginning at position 4 and continuing to the C terminus.

Comparing the peptide in the TCR–pMHC complex with the peptide in the unbound NS3/A2 (PDB ID 3MRM) complex indicates that there are no major alterations to peptide confor-

mation upon TCR binding. Interestingly, however, the latter portion of the peptide is "lifted" from the binding groove by 1–1.5 Å upon TCR binding, beginning at p4 Ala and continuing through the C-terminal valine at p10 (Fig. 3*C*). Peptide lifting is not attributable to weak peptide binding to the MHC, because NS3 binds strongly to A2 as shown above. It may reflect the weaker participation of the β-chain in engaging the peptide, perhaps coupled with weaker interactions of peptides with class I MHC proteins at their C-terminal ends (29).

HCV1406 Engagement of HLA-A2. Although peptide engagement is biased toward the N-terminal half as discussed above, the HCV1406 TCR binds the A2 protein centrally, making contacts along the α1- and α2-helices. On the α1-helix, salt-bridges from Glu34 in CDR1α and Glu101 in CDR3α neutralize the positively charged cluster of Arg65 and Lys66 (Fig. 4 *A* and *C*). The Arg65/Lys66 combination is essentially exclusive to A2, and the engagement of this region via electrostatic interactions from CDR1α and CDR3α is a distinctive feature of TCRs that bind A2, influencing the position of the TCR as well as the composition of TCR loops (30).

Further down the α1-helix, the region from Ala69 to Val76 is contacted by CDR2β, whose hairpin structure runs almost parallel to the helix (Fig. 4 *B* and *C*). Tyr50 of CDR2β is aligned alongside the helix as commonly observed in many TCR–pMHC complexes (31), contacting Ala69 and Gln72. Glu56β forms a salt-bridge with Arg75, an interaction less frequently observed in TCR complexes but present in several structures of TCRs with A2 (30).

Contacts to the α2-helix are more distributed among the TCR-binding loops, with residues in CDR1α, CDR2α, CDR1β, and CDR3β all engaging a span of the helix that ranges from Lys146 in the short arm to Thr163 in the long arm (Fig. 4 *D* and *E*). There are multiple electrostatic interactions between the TCR and the length of the α2-helix. These interactions include a salt-bridge from Asp30 of CDR1β to Lys146, which is also observed in other complexes with A2 (30). Another salt-bridge is formed between Lys60 of CDR2α and Glu154, and hydrogen bonds are made to Ala149 and Thr163 from residues in CDR3β and CDR1α, respectively.

Structural Features of Allorecognition: Recognition Is Dependent on Surface Features that Distinguish A2 from Other MHC Proteins in the Host. Although it recognizes NS3 presented by A2, the HCV1406 TCR developed in a host that was HLA-A2⁻. To gain more insight into the basis for allorecognition of HLA-A2 by HCV1406, we compared the sequences of A2 with the sequences of other class I HLA proteins, emphasizing those amino acids that were contacted by the TCR or otherwise likely to influence receptor binding. Our goal was to isolate any distinctive features of A2 compared with host class I molecules on which HCV1406 may have been positively selected or otherwise engaged during the course of its normal biology, and then to ascertain the extent to which the TCR relied upon these A2-distinctive features for binding. We also assessed the importance of these positions on the peptide–MHC interaction.

We first compared A2 with the classical class I MHC proteins of the allograft recipient, which were typed as A3/A30 and B7/B13 for HLA-A and HLA-B. The HLA-C genes in the host were not recorded, but the C family is less polymorphic and we were able to assess all known C types. Fifty polymorphic sites in human class I MHC proteins are found in the peptide-binding domain. For the A, B, and C alleles, 16 of these alleles are in the α1-helix and seven are in the α2-helix. Most of the polymorphic sites are outside of the contact zone of the TCR. Nonetheless, after examining the sequences in the context of the structure, it was clear that the binding of the HCV1406 TCR is directly influenced by sites that distinguish A2 from the other class I MHC proteins.

The clearest influences of A2 polymorphic sites were seen on the more polymorphic α1-helix (Fig. 5*A*). Position 62 is a glycine in A2, but a glutamine or arginine in the other A and B proteins
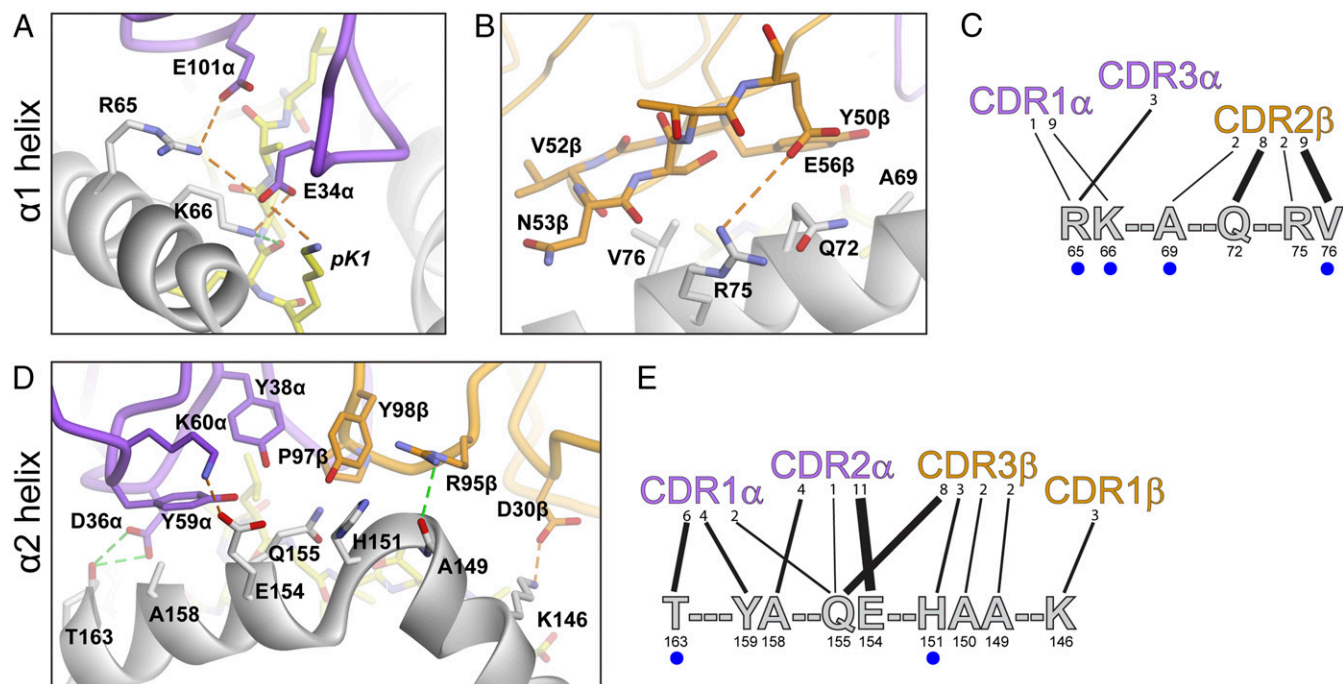
Fig. 4. Engagement of HLA-A2 by HCV1406. (*A*) As seen widely in other TCR structures with A2 (30), electrostatic interactions are formed between the TCR and N-terminal end of the A2 α1-helix. In addition to interacting with the peptide, Glu34 in CDR1α forms salt-bridges with Lys66 and Arg65. Glu101 in CDR3α forms a salt-bridge with Arg65. (*B*) CDR2β docks parallel to the C-terminal end of the α1-helix. A salt-bridge is formed between Glu56β and Arg75. (*C*) Schematic showing TCR contacts to the α1-helix by the participating CDR loops. The width of the black lines is proportional to the number of contacts, as indicated by the numbers above each line. The blue circles indicate polymorphic sites. (*D*) Interactions between the A2 α2-helix are more distributed, involving residues from CDR1α, CDR2α, CDR3β, and CDR1β. (*E*) Schematic showing TCR contacts to the α2-helix by the participating CDR loops. The width of the black lines is proportional to the number of contacts, as indicated by the numbers above each line. The blue circles indicate polymorphic sites.

and in >99% of the C proteins. HCV1406 does not directly contact Gly62, but the position is buried by the CDR1α loop in the structure of the complex, such that a glutamine or arginine would clash with Ser33α and Glu34α (Fig. 5*B*). Substitution of Gly62 with glutamine or arginine weakened the binding of HCV1406 to NS3/A2 between six- and 10-fold as measured by SPR (Fig. 5*A* and Table 2; data in Fig. S3).

Further down the α1-helix, Arg65 and Lys66 form the cluster of positive charge that is almost exclusive to A2 and helps orient A2-binding TCRs on the MHC (30). Arg65 is glutamine in the B proteins and in >99% of the C proteins, and Lys66 is asparagine in the other A proteins and isoleucine in the B proteins. In the HCV1406 structure, Arg65 forms salt-bridges with Glu101 of CDR3α and Glu34 of CDR1α, and Lys66 forms a salt-bridge with Glu34α (Fig. 5*C*). Modeling glutamine in for Arg65 or asparagine/isoleucine in for Lys66 did not introduce any inter-atomic clashes, but these replacements would disrupt the network of electrostatic interactions linking the TCR and its ligand. Substitution of Arg65 with the glutamine found in the B or C proteins had a dramatic impact on TCR binding, leading to undetectable binding (Table 2). Similar results were obtained when Lys66 was substituted with the asparagine found in A3/A30 or the isoleucine found in B7/B13. The R65Q/K66I double mutation also led to undetectable binding.

Other amino acids that are at least partially distinctive to A2 and are involved in the HCV1406 interface are Ala69, Val76, and Gly79. Position 69 is arginine in the C proteins, position 76 is glutamate in the B7/B13 proteins, and position 79 is arginine in the B7/B13 and C proteins. Mutations at these positions would introduce clashes (A69R), charge repulsion (V76E), or both (G79R) (Fig. 5 *D–F*). As predicted, mutations at these sites also had disruptive effects on TCR binding (Fig. 5*A* and Table 2).

We identified rare variants of the A, B, and C proteins that had some of the surface features noted above (i.e., C*02:66 has the R65/K66 pair), but none had all. We also examined the less

polymorphic nonclassical class I MHC proteins, and found that HCV1406 interacts with elements of the A2 surface that distinguish it from these rare variants as well. For example, variants of the nonclassical class I molecules HLA-E, HLA-F, and HLA-G lack glycines at positions 62 and 79 and the positive charge cluster of Arg65/Lys66 (Fig. 5*A*).

Although the TCR clearly interacted with sites that are distinctive to A2, it did not show preferential engagement of polymorphic sites at the expense of others, because nonpolymorphic sites made significant contacts, as shown in Fig. 4 (major nonpolymorphic contact sites include Gln72 on the α1-helix and the stretch of Glu154 to Tyr159 on the α2-helix). Moreover, other polymorphic sites did not seem to play a direct role in TCR binding. One example is position 151 on the α2-helix. Position 151 is a histidine in A2, but an arginine in A30 and the B/C proteins. In the structure of the HCV1406 complex, there are contacts between the His151 side chain and the ring of Tyr98 of CDR3β (Fig. 5*G*). Modeling arginine in the place of His151 would not remove these contacts, or introduce any other clashes. Consistent with the structure, mutation of His151 to arginine had no discernable impact on TCR binding (Table 2 and Fig. S3).

We also compared the sequence of A2 with class II MHC sequences because it is possible that T cells expressing HCV1406 were positively selected on a class II protein. Although class I and class II proteins are structurally homologous, they are sufficiently different at a local level to conclude that A2 presents a surface distinct from any class II MHC proteins in the host. For example, the lengths and twists of the class I/class II peptide-binding groove α-helices differ, as do the identity of the polymorphic and nonpolymorphic sites across the two helices. At a more granular level of detail, no human class II MHC α-chains maintain those features most distinctive to A2 at the equivalent positions in the peptide-binding domain α-helices (e.g., Gly62, Arg65/Lys66).
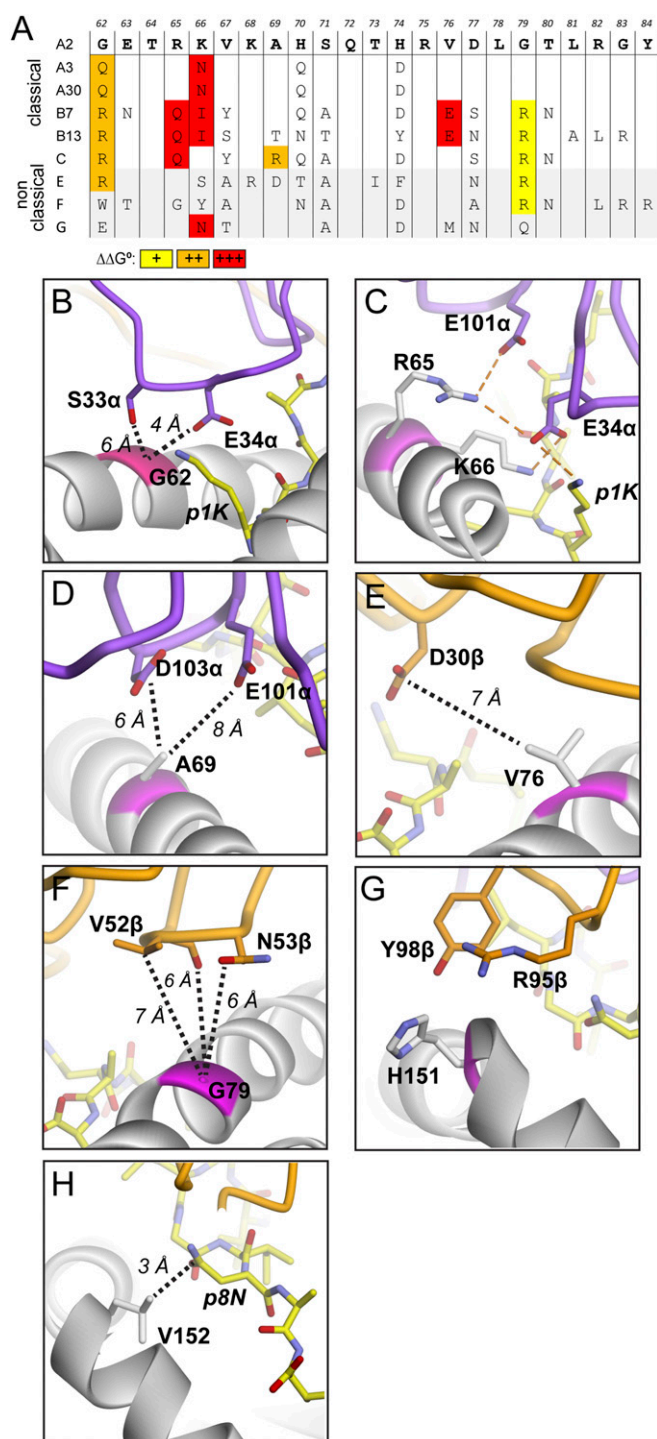
Fig. 5. Structural features of allorecognition of HLA-A2 by HCV1406. (*A*) Sequences of the α1-helix for the HLA-A2, HLA-A3, HLA-A30, HLA-B7, HLA-B13, HLA-C, HLA-E, HLA-F, and HLA-G families. The A2 sequence is across the top; differences from the other alleles identified via the IMGT database are noted. Mutations designed to test the importance of A2 surface features on receptor binding are shaded yellow, orange, or red depending on their impact on ΔΔG° (values are provided in Table 2, and binding data are provided in Fig. S3). (*B*) Substitutions to Gly62 present in A2 would result in steric clashes with Ser33 and Glu34 of CDR1α. (*C*) Substitutions to the Arg65/Lys66 pair found in A2 would perturb finely tuned electrostatic interactions with the peptide, CDR1α, and CDR3α. (*D*) Substitution of Ala69 present in A2 with the arginine found in C proteins would result in clashes and charge repulsion with Asp103 and Glu101α of CDR3α. (*E*) Substitution of Val76 with the glutamate found in B7/B13 could result in clashes and charge repulsion with Asp30 of CDR1β. (*F*) Substitution of

Overall, our results confirm that binding of HCV1406 to NS3/A2 is strongly dependent upon select polymorphic surface residues that distinguish A2 from other MHC proteins within the host that received the A2+ allograft. This distinction includes all known variants of the alleles that were recorded upon transplantation (A3, A30, B7, and B13), as well as the unrecorded HLA-C, nonclassical class I, and class II proteins.

HLA-A2 Polymorphisms Impact Peptide Binding and Conformation and Indirectly Influence TCR Binding. The polymorphisms assessed above impacted receptor binding to various extents, but did not significantly impact peptide binding as measured by DSF (Table 2). Due to their positions within the peptide-binding groove, however, the majority of other A2 polymorphisms are expected to impact the MHC–peptide interaction. Impacts on peptide binding are obvious at a high level, because MHC polymorphisms dictate amino acid preferences, particularly at the primary anchors (18). The preferences among A2, A3, A30, B7, B13, and C alleles differ considerably. For example, A2 prefers a small hydrophobic amino acid, such as valine, at the peptide C terminus, whereas A3 prefers a positively charged amino acid, such as lysine. To help quantify the impact of the binding groove polymorphisms on peptide binding, we assessed the binding of the NS3 peptide to the other A, B, and C alleles using the consensus-based MHC-I–binding prediction server from the Immune Epitope Database (32). As expected, the NS3 peptide was predicted to be most strongly bound by A2 (Table S1).

Beyond impacting peptide binding directly, polymorphisms within the binding groove are also likely to influence peptide conformation, detectable as an impact on TCR-binding affinity (33, 34). We tested influences on conformation directly by examining position 152, which is a valine in A2 and B13, but a glutamate or tryptophan in the other A, B, C, and E proteins. Substituting in either the glutamate or the tryptophan is predicted to influence peptide conformation through clashes with Asn8 of the peptide (Fig. 5*H*). Indeed, replacing Val152 with glutamate weakened TCR binding approximately threefold, whereas replacing it with tryptophan led to much weaker binding (Table 2 and Fig. S3). These outcomes are consistent with alterations in peptide conformation. Of all those mutations tested, these mutations also had the greatest impact on peptide binding to the MHC as assessed by measurements of thermal stability (Table 2). These results confirm that in addition to impacting peptide and TCR binding directly, A2 polymorphisms can impact TCR binding indirectly via their influence on peptide conformation.

Cross-Reactivity with a Tumor Antigen Reveals Cooperativity Between Structural Mimicry and a Peptide Hot Spot. In examining the structure of the HCV1406–NS3/A2 complex, we noted that the conformation of the NS3 peptide in the A2-binding groove is remarkably similar to the conformation of the decameric MART-1 tumor antigen (sequence ELAGIGILTV) bound to A2 (35, 36) (Fig. 6*A*). In addition to the common backbones, except for the p1 residue, there are chemical and structural similarities in both peptide side chains. These similarities are best shown by a superimposition of the MART-1 peptide onto the NS3 peptide in the HCV1406–NS3/A2 complex (Fig. 6*B*). There are no steric clashes with the TCR or MHC, and key residues identified both structurally and functionally show structural and chemical compatibility (e.g., leucine/isoleucine at p5).

In the context of the structure, the only major difference between the two peptides is the p1 Lys in NS3 vs. the p1 Glu in MART-1. The p1 Lys forms multiple electrostatic interactions

Gly79 in A2 with the arginine found in B7, B13, C, E, and F proteins could result in clashes with Val52 and Asn53 of CDR2β. (*G*) Substitution of His151 present in A2 with the arginine found in the A30, B7, B13, and C proteins should have little impact on receptor binding. (*H*) Substitutions to Val152 present in A2 would perturb the peptide–MHC interaction via clashes with the P8 arginine.

Table 2. Impact of mutations at HLA-A2 polymorphic sites on TCR and peptide binding

HLA-A2 variant	K_d,* μM	$\Delta\Delta G°$,[†] kcal/mol	T_m,[‡] °C
Wild type	16 ± 1		63.5 ± 0.1
G62Q	100 ± 10	1.1	63.1 ± 0.2
G62R	164 ± 13	1.4	60.4 ± 0.3
R65Q	nbd[§]	>2[§]	62.6 ± 0.2
K66I	>300[¶]	>2	63.2 ± 0.2
K66N	>300[¶]	>2	63.2 ± 0.2
R65Q/K66I	nbd	>2	62.4 ± 0.1
A69R	154 ± 8	1.3	63.1 ± 0.3
V76E	nbd	>2	63.6 ± 0.1
G79R	77 ± 2	0.9	64.3 ± 0.1
H151R	15 ± 1	0	64.2 ± 0.1
V152E	46 ± 3	0.6	51.0 ± 0.2
V152W	>300[¶]	>2	55.4 ± 0.2

nbd, no binding detected.

*K_d for TCR binding to pMHC measured by SPR. Errors are SDs from three experiments.

[†]Change in binding free energy determined from $\Delta\Delta G° = RT\ln(K_{d,mutant}/K_{d,wild\ type})$.

[‡]Apparent T_m of the pMHC complex determined by DSF. Errors are SDs of four experiments.

[§]Change in $\Delta\Delta G°$ is estimated at greater than 2 kcal/mol based on established SPR measurement sensitivity (40).

[¶]Weak binding detected, but not quantifiable. Affinity is estimated at >300 μM.

with the TCR (Fig. 3), and their importance is demonstrated by the negative impact of the K1A substitution on binding and function (Fig. 1). As shown in Fig. 6B, superimposition of the MART-1 peptide into the HCV1406–NS3/A2 complex showed charge repulsion would occur between the p1 Glu of MART-1 and Glu34 of CDR1α, with a distance between the two carboxylates of only 3.5 Å.

The structural and chemical convergence between NS3 and MART-1, and how they fit within the interface between HCV1406 and A2, prompted us to ask if the HCV1406 TCR could recognize a variant of the MART-1 decamer modified at the N terminus to provide the crucial positive charge present in the NS3 peptide. Accordingly, we examined a MART-1 peptide with p1 Glu substituted with lysine (KLAGIGILTV). In a binding experiment with SPR, HCV1406 recognized this ligand with an affinity threefold weaker than the affinity toward the NS3 epitope (Fig. 6C). We saw no detectable binding with the wild-type MART-1 epitope. We also saw no detectable binding with a variant of the negative control tyrosinase peptide modified with a p1 Lys (KMDGTMSQV), demonstrating the importance of the NS3/MART-1 structural convergence in permitting TCR cross-reactivity. Consistent with the binding data, the p1-modified MART-1 peptide was also recognized by HCV1406 TCR-transduced T cells in a CD8-dependent manner, whereas no recognition of the native MART-1 peptide was observed (Fig. 6D). These results further demonstrate the crucial importance of unique peptide features in determining HCV1406 specificity, to include the p1 Lys "hot spot" and the conformation of the peptide in the groove. Moreover, they reinforce how peptide features work together with the distinctive surface chemistry of A2 in dictating the allospecific nature of the HCV1406 TCR.

Discussion

The drivers of TCR alloreactivity have been variously attributed to a TCR focus on unique allopeptides presented by allo-MHC (peptide-centric) or to a TCR misfocus on polymorphic amino acids on the α-helices of allo-MHC peptide-binding grooves (MHC-centric) (37–39). The surprising specificity of many alloreactive TCRs and structural studies of alloreactive complexes have challenged these theories (3, 12, 13). Highly specific alloreactive T cells and TCRs are being explored for targeting

what otherwise would be poorly immunogenic shared tumor antigens and have been adopted for treatment of posttransplantation-associated lymphoproliferative disease (4, 6, 7).

Here, we show that for the highly specific alloreactive TCR HCV1406, recognition is both peptide- and MHC-centric, with polymorphisms impacting how the TCR sees the MHC protein as well as how the peptide is bound and presented. The structure of the HCV1406–NS3/A2 complex revealed that the TCR engages with a traditional binding mode, geometrically near the limits but still within what has been observed for other TCR complexes with A2. The TCR contacts polymorphic and nonpolymorphic sites along the α-helices of the A2-binding groove, but does not focus solely on polymorphic sites, nor does it avoid them. Of note are how the TCR interfaces with features that are unique to A2, most notably the cluster of positive charge composed of arginine at position 65 and lysine at position 66. Electrostatic interactions with Arg65 and Lys66 are a characteristic signature of TCRs that bind A2 (30), and changing Arg65 or Lys66 to their counterparts in other human class I MHC proteins disrupts receptor binding without impacting peptide binding. Recognition is likewise influenced by other A2-distinctive features, such as the collective identity of positions 62, 69, 76, and 79. Thus, binding of HCV1406 is dependent upon features that distinguish the TCR-interacting surface of A2 from other MHC proteins, both classical and nonclassical class I as well as class II.

As seen in other systems (33, 34), other polymorphic sites within the A2 peptide-binding groove impact alloreactivity through influences on peptide selection as well as peptide conformation. Recognition also depends upon details of the NS3 peptide that are not influenced by polymorphisms. The defining example is the lysine at p1, which is engaged by residues of CDR1α and whose replacement with alanine substantially weakens binding and eliminates functional recognition.

Overall, the picture that emerges is that alloreactive recognition of NS3/A2 by HCV1406 is driven by three elements that, together, define the composite peptide/MHC surface: (i) the unique TCR contact surface of A2, including polymorphisms that distinguish it from other MHC proteins that HCV1406 may have encountered in its host; (ii) properties of the NS3 peptide that are influenced by polymorphisms within the peptide-binding groove; and (iii) structural and chemical properties of the NS3 peptide itself. Perturbation of any one of these elements alone is sufficient to weaken receptor binding substantially.

These results explain the allospecific nature of HCV1406, but are there lessons for alloreactivity in general? Our findings are consistent with fundamental studies on TCR recognition showing that TCR engagement of pMHC depends on unique surface chemistries provided by both the peptide and MHC, whose "roles" in binding are not easily separable (40). Our findings therefore echo suggestions that at the molecular level, TCR allorecognition is more "normal" than "abnormal" (3, 12). We do not argue that more fully peptide- or MHC-centric alloreactivity does not exist, but that perhaps we should not anticipate TCR allorecognition to be unusually distinctive. If such is the case, our results may also help explain the high frequency of alloreactive T cells, because the combination of different surface chemistries on allo-MHC, the influence of polymorphisms on peptide selection and conformation, and the presentation of unique peptides collectively provide for recognition surfaces quite distinctive from the recognition surfaces found syngeneically.

Our findings also offer perspectives on the determinants of TCR MHC restriction. MHC restriction has been proposed to emerge from the requirements for the CD4/CD8 coreceptors during thymic selection and T-cell signaling (41). Our data make it clear that if thymic education does select for MHC restriction, it is sufficiently "fuzzy" to permit TCR engagement of allo-MHC in standard geometries. Alloreactive TCRs such as HCV1406 that bind in standard geometries could underscore a need to form a competent TCR–pMHC signaling complex that is structurally compatible with the binding of coreceptor and/or CD3 signaling units (42). There is evidence that such structural requirements do
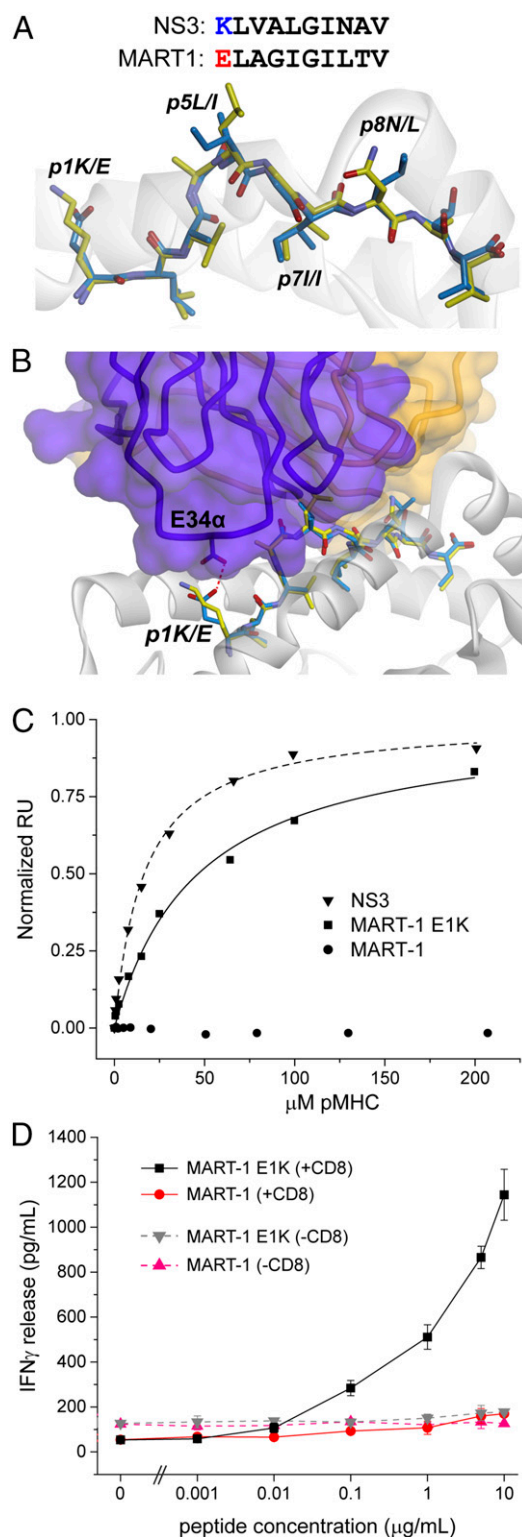
Fig. 6. Structural mimicry between the NS3 and MART-1 peptides. (*A*) Despite sequence differences, the MART-1 decamer peptide is a close structural and chemical mimic of the NS3 peptide, as shown in this superimposition of the MART-1 decamer from the MART-1/A2 complex onto the NS3 peptide in the HCV1406–NS3/A2 complex. The clearest difference is with the lysine (NS3) and glutamate (MART-1) at p1. (*B*) When the HCV1406 TCR is visualized in the superimposition, the receptor would clearly accommodate the MART-1 peptide. The only obvious incompatibility is the presence of glutamate instead of lysine at position 1, which would introduce charge repulsion with Glu34 of CDR1α, as shown with the red dashed line. (*C*) Consistent with

exist: In one instance, a TCR–pMHC complex with a highly unusual geometry did not signal (28), and, more recently, TCRs that bind with reverse polarity have been shown to lead to poor T-cell activation (26).

On the other hand, MHC restriction has been proposed to emerge from an intrinsic bias of TCRs toward MHC proteins (43), and there is evidence that TCR genes have coevolved with genes of the MHC (44). Our observations of a traditional binding mode with associated specificity could therefore reflect the influence of coevolved TCR-MHC contacts in binding. Indeed, the HCV1406–NS3/A2 complex displays the hallmarks of TCRs that bind A2, most notably the accommodation of the positive charges on Arg65 and Lys66. We recently presented evidence that, given the high frequency of A2 in human populations, the need to offset this charge cluster has influenced the composition of TCR genes, leading to biased recognition and restricted TCR positioning (30). Therefore, although geometrical requirements for coreceptor and CD3 compatibility could influence HCV1406 binding, the complex displays features associated with TCR-MHC coevolution and a subsequent inherent bias of TCRs for MHC proteins.

The fact that we could generate an HCV1406 cross-reactive peptide based not on the NS3 viral epitope but on the structural properties of the unrelated MART-1 tumor epitope underscores the importance of structural mimicry (as opposed to sequence mimicry) in T-cell recognition, both natural and allo. The observation that HCV1406 can cross-react between the NS3 epitope and a single amino acid variant of MART-1 may seem coincidental: Of the billions of possible decameric peptides, why would the well-studied MART-1 peptide be identified as the root of a molecular mimic? First, we note that in the central regions, MART-1 and NS3 are both rather featureless, lacking bulky or polar/charged side chains. Second, the backbone conformations of the peptides are nearly identical, which is not unusual with 9- and 10-mers bound to class I MHC proteins. Third, where the peptides are most different (p1 Lys in NS3 and p1 Glu in MART-1) is the exact region where substitutions have the greatest impact and direct cross-recognition. HCV1406 cross-reactivity with a modified MART-1 peptide therefore underscores the importance of hot spots in TCR specificity: The TCR engages a key region of the peptide that most directly influences specificity, restricting amino acid composition there but leaving other regions open to more diversity (45, 46). Our observations illustrate how hotspots can work alongside mimicry in directing TCR specificity/ cross-reactivity and reinforce how peptide features working alongside the distinctive surface chemistry of allo-MHC can drive allospecificity.

In conclusion, we have shown that the specificity of the HCV1406 TCR emerges from how the TCR engages the cooperative pMHC surface, with MHC polymorphisms influencing receptor binding directly via TCR-MHC contacts and indirectly via impacts on peptide binding and conformation. These observations can explain the paradox of TCR specificity in alloreactivity, and provide a structural and molecular context for the use of alloreactive TCRs in immunotherapy. More generally, our observations sharpen the discussion of how MHC restriction is achieved, and provide a clear example of how a peptide hotspot combined with structural mimicry can drive TCR cross-reactivity.

Methods

Cells, Media, and Reagents. The 293GP, PG13, T2, and Jurkat cell lines were obtained from the American Type Culture Collection. The 293GP cells were

the structural predictions, in a direct binding experiment, HCV1406 recognizes a variant of MART-1 with the p1 Glu substituted with lysine. No recognition was seen of the native MART-1 peptide, emphasizing the importance of the p1 Lys. Binding to NS3 from Fig. 1 is shown as a dashed line for comparison. (*D*) E1K-modified MART-1 peptide was also recognized in a functional assay by HCV1406-transduced CD8⁺ T cells, as shown in this titration assessing IFN-γ release.

maintained in DMEM supplemented with 10% FBS. The PG13 cells were maintained in Iscove's DMEM supplemented with 10% FBS. The T2 and Jurkat cell lines were maintained in RPMI medium 1640 supplemented with 10% FBS.

Generation of CD8+ Jurkat cells has been described previously (19, 47). Briefly, a modified SAMEN retroviral vector containing full-length human CD8 α and β, separated by an internal SRα promoter, and an internal ribosome entry site/neo^r cassette was used to transduce cells. CD8+ cells were sorted for high and uniform expression by FACS using anti–CD8-PerCP/Cy5.5 mAb and maintained in RPMI medium 1640 supplemented with 10% FBS and 500 μg/mL G418.

Human T cells were derived from deidentified apheresis products from normal, healthy donors, purchased from Key Biologics. Ficoll-Hypaque density gradient centrifugation was used to isolate peripheral blood mononuclear cells (PBMCs). Activated T cells used for retroviral transduction were generated by stimulating PBMCs with 50 ng/mL anti-CD3 mAb for 3 d in AIM-V medium supplemented with 5% heat-inactivated pooled human AB serum, 300 IU/mL recombinant human IL-2, and 100 ng/mL recombinant human IL-15.

As described in the original publication describing the HCV1406 TCR, HLA typing was performed using PCR amplification with sequence-specific primers (21). The original publication did not list the B types, but they were recorded at the time as HLA-B7 and HLA-B13.

Retroviral Transduction. Retroviral supernatants were prepared using a high-titer stable retroviral producer cell line, PG13, expressing HCV1406 TCR in a modified SAMEN retroviral vector. Retroviral vectors contained the TCR α-chain linked to the TCR β-chain and a truncated CD34 molecule by P2A and T2A self-cleaving sequences, respectively. Generation of these stable producer cell lines and collection of retrovirus have been described previously (20, 22).

Jurkat cells, CD8+ Jurkat cells, and anti–CD3-activated primary T cells were transduced to express HCV1406 TCR via spinoculation, as previously described (20, 22, 47, 48). Briefly, 0.5 mL per well of 30 μg/mL retronectin was used to coat 24-well, flat-bottom, nontissue culture-treated plates overnight at 4 °C. The next day, plates were blocked with 0.5 mL per well of 2% PBSA (PBS containing 2% BSA in PBS for 30 min at room temperature and washed with 2 mL per well of PBS). Plates were loaded with 2 mL per well of filtered retroviral supernatant, spun for 2 h at 2,000 × g at 32 °C, and gently aspirated. Two million Jurkat cells in 1 mL of RPMI/10% FBS or 2 million OKT3-activated T cells in 1 mL of AIM-V supplemented with 5% human immunoglobulin monoclonal antibody (hAB), 600 IU/mL recombinant human IL-2 (rhIL-2), and 200 ng/mL rhIL-15 were mixed with 1 mL per well of retroviral supernatant and added to each well. The plates were spun again for 2 h at 2000 × g at 32 °C. After 24 h, the transduced cells were harvested and transferred to tissue culture-treated flasks. Three days later, the cells were analyzed for transduction efficiency by FACS analysis using anti-CD34-phycoerythrin (PE) mAb. T cells or Jurkat cells were then sorted for TCR-transduced cells by positive selection using anti-CD34 mAb-coated immunomagnetic beads. TCR-transduced T cells were also sorted into CD4+ or CD8+ fractions using anti-CD4 and anti-CD8 mAb-coated immunomagnetic beads.

Immunofluorescence and Cytokine-Release Assays. HCV1406-TCR transduced Jurkat cells and T cells were evaluated for transduction efficiency via immunofluorescence staining and quantified via flow cytometry as previously described (20, 22). The mAbs used in these experiments were anti-CD3-APC/Cy7, anti-CD4-PE/Cy7, anti-CD8-PerCP/Cy5.5, and anti-CD34-PE. Flow cytometry was performed using a Canto II flow cytometer, and data were analyzed with FlowJoX (FlowJo, LLC).

Antigen reactivity by HCV1406 TCR-transduced T cells and Jurkat cells against peptide-loaded T2 cells was assessed by cytokine release assays as previously described (49). Briefly, T2 cells were pulsed with 10 μg/mL peptide for 2 h. For peptide titrations, T2 cells were pulsed with peptide concentrations ranging from 10–0.001 μg/mL. Target T2 (1×10^5) cells and effector (TCR-transduced T cells or Jurkat; 1×10^5) cells were cocultured in a 1:1 ratio in 96-well, U-bottom, tissue culture plates in 200 μL of RPMI 1640 supplemented with 10% FBS. Phorbol 12-myristate 13-acetate (10 ng/mL) was added to Jurkat cell cocultures to enhance sensitivity of stimulation as described elsewhere (20, 22). Cocultures were incubated at 37 °C overnight, supernatants were harvested, and the amount of IFN-γ or IL-2 released by 1×10^5 T cells or Jurkat cells, respectively, was measured by ELISA.

Peptides and Proteins. Soluble pMHC and TCR were refolded from bacterially expressed inclusion bodies following established procedures (50). Briefly, isolated inclusion bodies of HLA-A2 heavy chain, β_2m, TCR α-chain, and TCR β-chain were dissolved in 8 M urea. For MHC refolding, HLA-A2 heavy chain

and β_2m were diluted into MHC refolding buffer containing 100 mM Tris·HCl (pH 8.3), 400 mM L-arginine, 6.3 mM cysteamine, 3.7 mM cystamine, 2 mM EDTA, and 0.2 mM PMSF at a 1:3 molar ratio with excess peptide. For the TCR, α-chains and β-chains were diluted into 50 mM Tris·HCl (pH 8.3), 2.5 M urea, 6.3 mM cysteamine, 3.7 mM cystamine, 2 mM EDTA, and 0.2 mM PMSF with a 20% excess of α-chain. After incubation for 12 h at 4 °C with constant stirring, the mixtures were dialyzed against 10 mM Tris·HCl (pH 8.3) for 48 h. Refolded complexes were purified with anion exchange chromatography followed by size exclusion chromatography. Peptides were synthesized commercially by Synthetic Biomolecules or Genscript, and were obtained at 95% purity. Mutations in the HLA-A2 heavy chain were made using PCR-based mutagenesis.

Peptide-binding predictions were performed using the Immune Epitope Database analysis resource Consensus tool (32) which combines predictions from ANN (51–53), SMM (54), and Comblib (55). HLA sequences were compared using data from the IMGT database (56).

Protein Crystallization, Data Collection, Structure Refinement, and Analysis. Crystals of the HCV1406–NS3/A2 complex were grown in 13% vol/vol PEG 3350, 0.1 M sodium cacodylate (pH 6.1), 0.2 M ammonia sulfate, and 3% wt/vol 1,5-diaminopentane dihydrochloride at a protein concentration of 6 mg/mL at 20 °C. Crystallization was performed by hanging drop vapor diffusion. For cryoprotection, crystals were transferred into 20% glycerol/80% mother liquor for 30 s and immediately frozen in liquid nitrogen. Diffraction data were collected at the 22ID SERCAT beamline at the Advanced Photon Source (Argonne National Laboratories). Data were indexed, integrated, and scaled with the program XDS22. The complexes were solved by molecular replacement with Phaser (57) using the Protein Database (PDB) ID codes 3QEU and 3MRM as search models (58). Rigid body refinement followed by translation/libration/screw refinement was performed with Phenix and Refmac5 (59, 60). The twinning law "-h, -k, l" was determined by Xtriage and applied in the last round of refinement. Evaluation of the models and fitting to maps were performed with the program Coot. The model was checked in WHATIF and MolProbity to evaluate the structure during the refinement (61, 62). Atomic positioning was verified with a simulated annealing composite OMIT map calculated in Phenix. Density for the α3-domain of HLA-A2 was weak for both molecules in the asymmetrical unit, contributing to greater than typical Ramachandran deviations. The structure has been deposited into the PDB with ID code 5JZI. Analysis of hydrogen bonds and van der Waals contacts was performed with the PISA server, using a cutoff of 4 Å for contacts (63). Solvent-accessible surface areas were calculated using Discovery Studio with a probe radius of 1.4 Å. Superimpositions and modeling of clashes and compatibility were performed with Discovery Studio. TCR crossing and incident angles were calculated as previously described (64, 65).

SPR and DSF. Steady-state–binding experiments were performed on Biacore 3000 and T200 instruments in HBS-EP buffer containing 10 mM Hepes (pH 7.4), 150 mM NaCl, 3 mM EDTA, and 0.005% surfactant P20. The HCV1406 TCR was covalently coupled to a CM5 sensor chip via standard amine coupling. Equilibrium-binding experiments were performed by injecting 25 μL of pMHC at a flow rate of 5 μL·min⁻¹ over the concentration range of 0.5 to 200 μM. The responses at equilibrium were determined by averaging the signal over the final 10 s of the injection and subtracting the responses from identical injections over a blank flow cell. Experiments were performed at 25 °C. Data were processed with BiaEvaluation 4.1 and fit with OriginPro using a 1:1 binding model. For each experiment, all injections were repeated twice and the two datasets were fit globally (66). Each experiment was performed in triplicate, and the results were averaged for reporting values and errors.

DSF was performed as previously described (24), using an Applied Biosystems StepOnePlus RT-PCR instrument with the excitation and emission wavelengths set to 587 nm and 607 nm, respectively. Protein was dialyzed in 10 mM Hepes (pH 7.4), 150 mM NaCl, 3 mM EDTA, and 0.005% surfactant P20 at concentrations of 4 μM, 6 μM, 8 μM, and 10 μM. SYPRO orange (Invitrogen) was added at fivefold and 10-fold concentrations to each protein concentration with a total reaction volume of 20 μL. The temperature range spanned 25–95 °C, with a scan rate of 1 °C·min⁻¹. Data analysis was performed in OriginPro 9.0. Apparent T_m values were determined from the first derivative of the melting curve. The derivative curve was processed with the single-peak–fitting algorithm in OriginPro, fitting the peak to a Bigaussian function. The apparent T_m values were averaged for measurements at four concentrations. Errors are reported as the SD of the four measurements.

1. Suchin EJ, et al. (2001) Quantifying the frequency of alloreactive T cells in vivo: New answers to an old question. *J Immunol* 166:973–981.
2. Smith PA, Brunmark A, Jackson MR, Potter TA (1997) Peptide-independent recognition by alloreactive cytotoxic T lymphocytes (CTL). *J Exp Med* 185:1023–1033.
3. Felix NJ, Allen PM (2007) Specificity of T-cell alloreactivity. *Nat Rev Immunol* 7:942–953.
4. Kumari S, et al. (2014) Alloreactive cytotoxic T cells provide means to decipher the immunopeptidome and reveal a plethora of tumor-associated self-epitopes. *Proc Natl Acad Sci USA* 111:403–408.
5. Sadovnikova E, Stauss HJ (1996) Peptide-specific cytotoxic T lymphocytes restricted by nonself major histocompatibility complex class I molecules: reagents for tumor immunotherapy. *Proc Natl Acad Sci USA* 93:13114–13118.
6. Barker JN, et al. (2010) Successful treatment of EBV-associated posttransplantation lymphoma after cord blood transplantation using third-party EBV-specific cytotoxic T lymphocytes. *Blood* 116:5045–5049.
7. Cooper LJN (2010) Off-the-shelf T-cell therapy. *Blood* 116:4741–4743.
8. Colf LA, et al. (2007) How a single T cell receptor recognizes both self and foreign MHC. *Cell* 129:135–146.
9. Garcia KC, et al. (1998) Structural basis of plasticity in T cell receptor recognition of a self peptide-MHC antigen. *Science* 279:1166–1172.
10. Hennecke J, Wiley DC (2002) Structure of a complex of the human alpha/beta T cell receptor (TCR) HA1.7, influenza hemagglutinin peptide, and major histocompatibility complex class II molecule, HLA-DR4 (DRA*0101 and DRB1*0401): insight into TCR cross-restriction and alloreactivity. *J Exp Med* 195:571–581.
11. Reiser JB, et al. (2003) CDR3 loop flexibility contributes to the degeneracy of TCR recognition. *Nat Immunol* 4:241–247.
12. Ely LK, Burrows SR, Purcell AW, Rossjohn J, McCluskey J (2008) T-cells behaving badly: Structural insights into alloreactivity and autoimmunity. *Curr Opin Immunol* 20:575–580.
13. Archbold JK, Macdonald WA, Burrows SR, Rossjohn J, McCluskey J (2008) T-cell allorecognition: A case of mistaken identity or déjà vu? *Trends Immunol* 29:220–226.
14. Macdonald WA, et al. (2009) T cell allorecognition via molecular mimicry. *Immunity* 31:897–908.
15. Kjer-Nielsen L, et al. (2003) A structural basis for the selection of dominant alphabeta T cell receptors in antiviral immunity. *Immunity* 18:53–64.
16. Simpson AA, et al. (2011) Structural and energetic evidence for highly peptide-specific tumor antigen targeting via allo-MHC restriction. *Proc Natl Acad Sci USA* 108:21176–21181.
17. Harjanto S, Ng LFP, Tong JC (2014) Clustering HLA class I superfamilies using structural interaction patterns. *PLoS One* 9:e86655.
18. Sidney J, Peters B, Frahm N, Brander C, Sette A (2008) HLA class I supertypes: A revised and updated classification. *BMC Immunol* 9:1.
19. Callender GG, et al. (2006) Identification of a hepatitis C virus-reactive T cell receptor that does not require CD8 for target cell recognition. *Hepatology* 43:973–981.
20. Spear TT, et al. (2016) Hepatitis C virus-cross-reactive TCR gene-modified T cells: A model for immunotherapy against diseases with genomic instability. *J Leukoc Biol* 100:545–557.
21. Rosen HR, et al. (2004) Cutting edge: Identification of hepatitis C virus-specific CD8+ T cells restricted by donor HLA alleles following liver transplantation. *J Immunol* 173:5355–5359.
22. Spear TT, et al. (2016) TCR gene-modified T cells can efficiently treat established hepatitis C-associated hepatocellular carcinoma tumors. *Cancer Immunol Immunother* 65:293–304.
23. Laugel B, et al. (2007) Different T cell receptor affinity thresholds and CD8 coreceptor dependence govern cytotoxic T lymphocyte activation and tetramer binding properties. *J Biol Chem* 282:23799–23810.
24. Hellman LM, et al. (2016) Differential scanning fluorimetry based assessments of the thermal and kinetic stability of peptide-MHC complexes. *J Immunol Methods* 432:95–101.
25. Birnbaum ME, et al. (2014) Deconstructing the peptide-MHC specificity of T cell recognition. *Cell* 157:1073–1087.
26. Gras S, et al. (2016) Reversed T Cell receptor docking on a major histocompatibility class I complex limits involvement in the immune response. *Immunity* 45:749–760.
27. Beringer DX, et al. (2015) T cell receptor reversed polarity recognition of a self-antigen major histocompatibility complex. *Nat Immunol* 16:1153–1161.
28. Adams JJ, et al. (2011) T cell receptor signaling is limited by docking geometry to peptide-major histocompatibility complex. *Immunity* 35:681–693.
29. Zacharias M, Springer S (2004) Conformational flexibility of the MHC class I alpha1-alpha2 domain in peptide bound and free states: A molecular dynamics simulation study. *Biophys J* 87:2203–2214.
30. Blevins SJ, et al. (2016) How structural adaptability exists alongside HLA-A2 bias in the human αβ TCR repertoire. *Proc Natl Acad Sci USA* 113:E1276–E1285.
31. Marrack P, Scott-Browne JP, Dai S, Gapin L, Kappler JW (2008) Evolutionarily conserved amino acids that control TCR-MHC interaction. *Annu Rev Immunol* 26:171–203.
32. Fleri W, et al. (2017) The immune epitope database and analysis resource in epitope discovery and synthetic vaccine design. *Front Immunol* 8:278.
33. Macdonald WA, et al. (2003) A naturally selected dimorphism within the HLA-B44 supertype alters class I structure, peptide repertoire, and T cell recognition. *J Exp Med* 198:679–691.
34. Hülsmeyer M, et al. (2004) Dual, HLA-B27 subtype-dependent conformation of a self-peptide. *J Exp Med* 199:271–281.
35. Borbulevych OY, et al. (2007) Structures of MART-126/27-35 Peptide/HLA-A2 complexes reveal a remarkable disconnect between antigen structural homology and T cell recognition. *J Mol Biol* 372:1123–1136.
36. Sliz P, et al. (2001) Crystal structures of two closely related but antigenically distinct HLA-A2/melanocyte-melanoma tumor-antigen peptide complexes. *J Immunol* 167:3276–3284.
37. Boardman DA, Jacob J, Smyth LA, Lombardi G, Lechler RI (2016) What is direct allorecognition? *Curr Transplant Rep* 3:275–283.
38. Bevan MJ (1984) High determinant density may explain the phenomenon of alloreactivity. *Immunol Today* 5:128–130.
39. Matzinger P, Bevan MJ (1977) Hypothesis: Why do so many lymphocytes respond to major histocompatibility antigens? *Cell Immunol* 29:1–5.
40. Piepenbrink KH, Blevins SJ, Scott DR, Baker BM (2013) The basis for limited specificity and MHC restriction in a T cell receptor interface. *Nat Commun* 4:1948.
41. Van Laethem F, Tikhonova AN, Singer A (2012) MHC restriction is imposed on a diverse T cell receptor repertoire by CD4 and CD8 co-receptors during thymic selection. *Trends Immunol* 33:437–441.
42. Rangarajan S, Mariuzza RA (2014) T cell receptor bias for MHC: Co-evolution or co-receptors? *Cell Mol Life Sci* 71:3059–3068.
43. Garcia KC (2012) Reconciling views on T cell receptor germline bias for MHC. *Trends Immunol* 33:429–436.
44. Sharon E, et al. (2016) Genetic variation in MHC proteins is associated with T cell receptor expression biases. *Nat Genet* 48:995–1002.
45. Adams JJ, et al. (2016) Structural interplay between germline interactions and adaptive recognition determines the bandwidth of TCR-peptide-MHC cross-reactivity. *Nat Immunol* 17:87–94.
46. Cole DK, et al. (2016) Hotspot autoimmune T cell receptor binding underlies pathogen and insulin peptide cross-reactivity. *J Clin Invest* 126:2191–2204.
47. Lyons GE, et al. (2006) Influence of human CD8 on antigen recognition by T-cell receptor-transduced cells. *Cancer Res* 66:11455–11461.
48. Clay TM, et al. (1999) Efficient transfer of a tumor antigen-reactive TCR to human peripheral blood lymphocytes confers anti-tumor reactivity. *J Immunol* 163:507–513.
49. Cole DJ, et al. (1995) Characterization of the functional specificity of a cloned T-cell receptor heterodimer recognizing the MART-1 melanoma antigen. *Cancer Res* 55:748–752.
50. Davis-Harrison RL, Armstrong KM, Baker BM (2005) Two different T cell receptors use different thermodynamic strategies to recognize the same peptide/MHC ligand. *J Mol Biol* 346:533–550.
51. Nielsen M, et al. (2003) Reliable prediction of T-cell epitopes using neural networks with novel sequence representations. *Protein Sci* 12:1007–1017.
52. Lundegaard C, et al. (2008) NetMHC-3.0: Accurate web accessible predictions of human, mouse and monkey MHC class I affinities for peptides of length 8–11. *Nucleic Acid Res* 36:W509–W512.
53. Andreatta M, Nielsen M (2016) Gapped sequence alignment using artificial neural networks: Application to the MHC class I system. *Bioinformatics* 32:511–517.
54. Peters B, Sette A (2005) Generating quantitative models describing the sequence specificity of biological processes with the stabilized matrix method. *BMC Bioinformatics* 6:132.
55. Sidney J, et al. (2008) Quantitative peptide binding motifs for 19 human and mouse MHC class I molecules derived using positional scanning combinatorial peptide libraries. *Immunome Res* 4:2.
56. Robinson J, et al. (2011) The IMGT/HLA database. *Nucleic Acids Res* 39:D1171–D1176.
57. McCoy AJ, et al. (2007) Phaser crystallographic software. *J Appl Cryst* 40:658–674.
58. Borbulevych OY, Santhanagopolan SM, Hossain M, Baker BM (2011) TCRs used in cancer gene therapy cross-react with MART-1/Melan-A tumor antigens via distinct mechanisms. *J Immunol* 187:2453–2463.
59. Winn MD, Isupov MN, Murshudov GN (2001) Use of TLS parameters to model anisotropic displacements in macromolecular refinement. *Acta Crystallogr D Biol Crystallogr* 57:122–133.
60. Adams PD, et al. (2011) The Phenix software for automated determination of macromolecular structures. *Methods* 55:94–106.
61. Vriend G (1990) WHAT IF: A molecular modeling and drug design program. *J Mol Graph* 8:52–56, 29.
62. Chen VB, et al. (2010) MolProbity: All-atom structure validation for macromolecular crystallography. *Acta Crystallogr D Biol Crystallogr* 66:12–21.
63. Krissinel E, Henrick K (2007) Inference of macromolecular assemblies from crystalline state. *J Mol Biol* 372:774–797.
64. Pierce BG, Vreven T, Weng Z (2014) Modeling T cell receptor recognition of CD1-lipid and MR1-metabolite complexes. *BMC Bioinformatics* 15:319.
65. Rudolph MG, Stanfield RL, Wilson IA (2006) How TCRs bind MHCs, peptides, and coreceptors. *Annu Rev Immunol* 24:419–466.
66. Piepenbrink KH, Gloor BE, Armstrong KM, Baker BM (2009) Methods for quantifying T cell receptor binding affinities and thermodynamics. *Methods Enzymol* 466:359–381.